

Magnetic anisotropy in the ferromagnetic Cu-doped ZnO nanoneedles

T. S. Heng, S. P. Lau,^{a)} S. F. Yu, and H. Y. Yang

School of Electrical and Electronic Engineering, Nanyang Technological University, Nanyang Avenue, Singapore 639798, Singapore

L. Wang

School of Physical and Mathematical Sciences, Nanyang Technological University, 1 Nanyang Walk, Singapore 637616, Singapore

M. Tanemura

Department of Environmental Technology, Graduate School of Engineering, Nagoya Institute of Technology, Gokiso-cho, Showa-ku, Nagoya 466-8555, Japan

J. S. Chen

Data Storage Institute, 5 Engineering Drive 1, Singapore 117608, Singapore and Department of Material Science and Engineering, National University of Singapore, Singapore 119260, Singapore

(Received 19 October 2006; accepted 17 December 2006; published online 19 January 2007)

Copper-doped ZnO (ZnO:Cu) nanoneedles exhibiting room-temperature ferromagnetism were fabricated by an ion beam technique using Cu plate and ZnO film. A saturated magnetization moment of 0.698 emu/cm^3 was found in the nanoneedles when a field of 10 kOe was applied perpendicular to the substrate, which was 15% larger than the field applied parallel to the substrate. The magnetic ordering of the nanoneedles was enhanced significantly to 0.968 emu/cm^3 after annealing of 400°C for 20 min. However, the magnetic anisotropy at high field is vanished but an “easy plane” ferromagnetism becomes apparent at low field region. The possible mechanisms of the magnetic ordering and anisotropy in the ZnO:Cu nanoneedles are discussed. © 2007 American Institute of Physics. [DOI: [10.1063/1.2433028](https://doi.org/10.1063/1.2433028)]

The prospects of integrating intrinsic magnetic and electronic functionalities into a single material have provoked intense interest towards developing wide band gap diluted magnetic semiconductor (DMS) system with room temperature (RT) ferromagnetism. Copper-doped ZnO (ZnO:Cu) is an unambiguous DMS as Cu and Cu-related precipitates are nonferromagnetic.¹ Recent theoretical and experimental studies have reported RT ferromagnetism in ZnO:Cu.¹⁻³ However, to date, most of the research on ferromagnetic ZnO:Cu focused on thin films and bulk materials. Nanostructured DMSs are expected to have a longer coherence time, which may provide a pathway for increasing the spin lifetime for practical spintronics applications.⁴ In this letter, we report the magnetic anisotropy in the ferromagnetic ZnO:Cu nanoneedles prepared by the ion beam technique at RT. This approach should shed light to the selective growth of DMSs on any substrate for functional spintronics devices.

ZnO and ZnO:Cu films with thicknesses of 850 and 1100 nm, respectively, were prepared on Si substrates at RT by the filtered cathodic vacuum arc (FCVA) technique. The details of FCVA apparatus have been described elsewhere.⁵ High purity (99.99%) Zn and $\text{Zn}_{99}\text{Cu}_1$ alloy (i.e., 1 at. % of Cu) targets were used as the cathode material for the growth of ZnO and ZnO:Cu films, respectively. Oxygen was used as reactant gas with flow rate of 60 SCCM (SCCM denotes cubic centimeter per minute at STP). Prior to the fabrication of nanoneedles, a thin layer of carbon was deposited onto the sample in order to enhance the ion-induced formation of nanoneedles.⁶ A Cu plate (99.99% purity) serving as Cu source during ion beam irradiation was placed perpendicular

to the ZnO sample. An ion beam source with 1 keV Ar^+ ions was irradiated at an incidence angle of 45° to the Cu and the ZnO surface for 4 min inside a vacuum system. Simultaneously, Cu was doped into the host material during nanoneedle formation. In order to compare the effectiveness of this method for doping, ZnO:Cu nanoneedles were also prepared by the similar ion beam technique but the starting material was a FCVA-deposited ferromagnetic ZnO:Cu film.¹ In this case, no Cu plate was used in the ion beam irradiation. After the fabrication of nanoneedles, the residue carbon layer was removed by ethanol prior to characterization. The ZnO:Cu nanoneedle samples were labeled as N1 and N2 for the ZnO and ZnO:Cu films used as starting materials, respectively.

The magnetic properties of samples were investigated by an alternating gradient magnetometer with a maximum field of 10 kOe. The structural properties of samples were studied by x-ray diffraction (XRD), scanning electron microscopy (SEM), transmission electron microscopy (TEM), and selected area electron diffraction (SAED) pattern. SAED ring patterns were simulated using the computer program JECPCED.⁷ The Cu contents in samples N1 and N2 were estimated to be $\sim 2.1\%$ and $\sim 1.3\%$, respectively, by the energy dispersive x-ray spectroscopy attached in the SEM.

The surface morphology and structural properties of sample N1 are presented here, as sample N2 exhibited similar structural properties of N1. The typical ZnO:Cu nanoneedle array is shown in Fig. 1(a). The lengths of the conelike structures ranged from 250 to 500 nm. The nanoneedles are oriented around $\sim 45^\circ$ to the substrate, which is similar to the ion beam irradiation direction. The average diameter of the nanoneedles in the stem part was $\sim 100 \text{ nm}$ with considerably sharp morphology as illustrated in Fig. 1(b). Figure 1(c) shows a well oriented (0002) plane of an individual nanon-

^{a)} Author to whom correspondence should be addressed; electronic mail: esplau@ntu.edu.sg

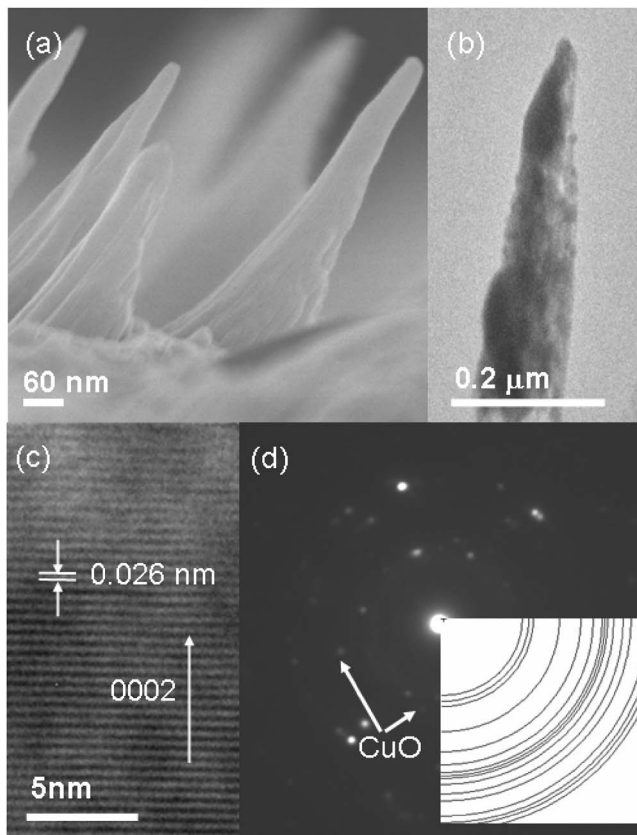


FIG. 1. (a) A typical cross-sectional SEM image of ZnO:Cu nanoneedles (sample N1). (b) TEM image of a ZnO:Cu nanoneedle and its corresponding high resolution TEM image is shown in (c). (d) Comparison of the SAED patterns of ZnO:Cu nanoneedles with the simulated patterns of ZnO. Some weak diffraction spots related to CuO were detected.

eedle with its interplanar distance of 0.26 nm, suggesting high crystallinity of the ZnO:Cu nanoneedles. Figure 1(d) shows the SAED patterns of a nanoneedle, and the inset is a simulated SAED ring pattern of ZnO. The SAED pattern of the nanoneedle is matched with the simulated ZnO pattern, implying that the nanoneedle exhibited the ZnO wurtzite structure. However, some weak diffraction spots of CuO could be seen in the pattern.

Figure 2 shows the XRD spectra of as-grown ZnO, ZnO:Cu, N1, and N2. All samples exhibited prominent (002) peak corresponding to ZnO wurtzite structure. The degradation of XRD intensities is observed with the incorporation of Cu into ZnO, elucidating the increase in structural disorder. It is because the incorporation of 3d transition ions, such as Cu, generally deteriorates the crystallinity of ZnO due to their low solubility and various valence states. Although sample N1 exhibited higher Cu content than N2, the XRD peak intensity of N1 is higher than that of N2. This discrepancy may be attributed to the crystal quality of the starting material as the XRD peak intensity of ZnO film is stronger than ZnO:Cu. As shown in the inset of Fig. 2, the (002) peak of the nanoneedles were shifted to higher angles by 0.02° – 0.06° as compared to that of ZnO film ($2\theta=34.34^\circ$), indicating the reduction of lattice parameter c . It is attributed to the substitution of the smaller Cu^{2+} ions into Zn^{2+} sites as Cu^{2+} ions have radii of 0.057 nm as compared to 0.06 nm for Zn^{2+} ions.⁸

Figure 3 shows the typical magnetization curves of sample N1. A well defined hysteresis behavior is observed

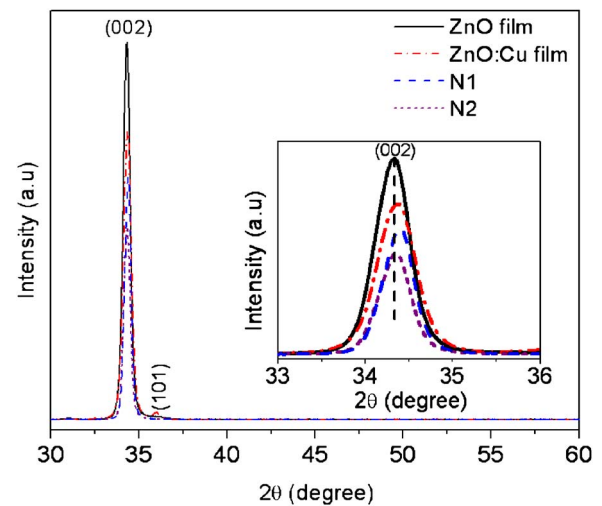


FIG. 2. (Color online) XRD pattern of ZnO film, ZnO:Cu film, and as-fabricated ZnO:Cu nanoneedles on Si (100) substrate. Inset shows an enlarged (002) peak of ZnO:Cu samples.

in the ZnO:Cu nanoneedles, magnetic ordering with coercivity (H_c), and saturated magnetization of 100 Oe and 0.698 emu/cm^3 , respectively, when the magnetic field was applied perpendicular to the substrate. The saturated magnetization of all samples measured with magnetic field applied parallel (M_s^{\parallel}) and perpendicular (M_s^{\perp}) to the substrate at 10 kOe is listed in Table I. The M_s^{\perp} of sample N2 is about 19% less than N1. Since the M_s values have been normalized by the volume of the thin film or nanoneedles, the difference of M_s^{\perp} between samples N1 and N2 may be attributed to the higher Cu content in sample N1 than in N2. It is noted that the M_s^{\perp} of N2 is 15% less than that of the ZnO:Cu film; the interfacial defects created by the ion beam irradiation and the orientation of the ZnO:Cu nanoneedles may be attributed to the reduction of the M_s^{\perp} after irradiation. It seems that ion beam irradiation is an effective method in doping Cu into ZnO and making it ferromagnetic.

The magnetic anisotropy in transition element substituted ZnO is a common characteristic of DMSs.⁹ Sati *et al.* reported that the magnetic anisotropy in ZnO:Co could be

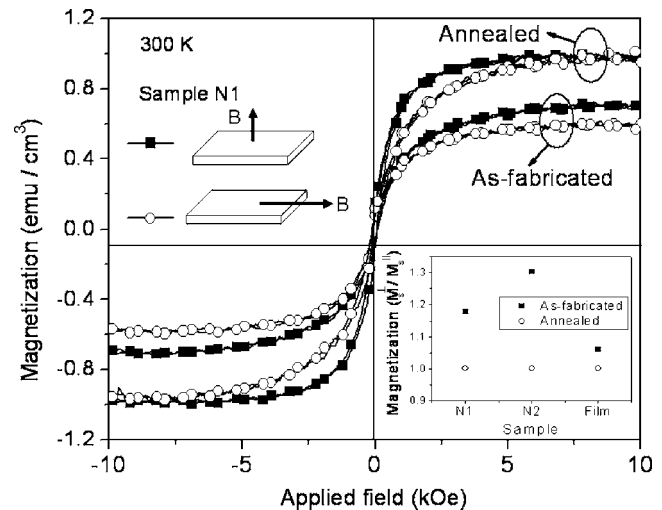
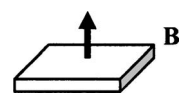



FIG. 3. Magnetization hysteresis loops of as-fabricated and annealed ZnO:Cu nanoneedles for sample N1 measured at 300 K. Inset shows the magnetization ratio $M_s^{\perp}/M_s^{\parallel}$ before and after annealing for samples N1, N2, and ZnO:Cu film.

TABLE I. The saturated magnetization of as-fabricated and annealed samples N1, N2, and ZnO:Cu film measured at applied field of 10 kOe.

Applied magnetic field direction	Sample N1 (emu/cm ³)		Sample N2 (emu/cm ³)		ZnO:Cu film (emu/cm ³)	
	As-fabricated	Annealed	As-fabricated	Annealed	As-grown	Annealed
	0.698	0.968	0.562	0.773	0.665	1.249
	0.593	0.966	0.431	0.773	0.628	1.242

considered as a signature of intrinsic ferromagnetism.¹⁰ Thus the magnetic anisotropy of the ZnO:Cu nanoneedle and thin film samples were studied. As shown in the inset of Fig. 3, the ratio M_s^\perp/M_s^\parallel for the three samples is greater than 1, indicating the anisotropy nature of the samples. The anisotropy of the M_s^\perp in the ZnO:Cu nanoneedles can be 30% larger than M_s^\parallel . The stronger anisotropy of the ZnO:Cu nanoneedles as compared to the thin film sample could be due to the shape and orientation of the nanoneedles as the nanoneedles are oriented $\sim 45^\circ$ to the substrate. In order to verify whether the shape or orientation of the nanoneedles will play a role in the anisotropy, the samples were annealed at 400 °C for 20 min. Under these optimal annealing conditions, the M_s^\perp of the ZnO thin films will be the highest ($M_s^\perp = 1.2$ emu/cm³). It is not clear why such conditions will give the highest M_s^\perp , but it may be related to the defect density of the sample as certain critical defect density will lead to the optimized magnetic couplings.¹¹ Surprisingly, after annealing the magnetization ratio M_s^\perp/M_s^\parallel of all the samples is equal to ~ 1 at the applied field of 10 kOe, as shown in the inset of Fig. 3. However, it should be noted that “easy plane” ferromagnetism can still be observed in all the samples at applied field less than 5 kOe. The typical magnetization curve of the annealed sample N1 is shown in Fig. 3. The easy plane is along the perpendicular axis of the substrate, which may be attributed to the magnetocrystalline anisotropy in our samples as they are predominately (002) oriented. The structural properties of the three annealed samples have been examined by XRD and SEM but no obvious difference can be observed in terms of XRD peak positions and surface morphology as compared to the as-fabricated samples. Thus, the changes of the magnetization ratio M_s^\perp/M_s^\parallel after annealing are unlikely related to the structural properties of the samples. In addition, the anisotropy of the samples at high applied field does not seem to be due to the shape and orientation of the nanoneedles. The mild but optimized annealing conditions has a significant effect on the saturated magnetization and anisotropy of the samples. The annealing temperature of 400 °C should be sufficient to redistribute inhomogeneous Cu²⁺ ions in ZnO since our samples were prepared under nonequilibrium condition (i.e., low growth temperature). A homogeneous distribution of Cu²⁺ ions in ZnO would favor ferromagnetism and it should lead to enhanced magnetization. On the other hand, the intrinsic defects in ZnO such as O vacancies and Zn interstitials (Zn_i) may be affected by annealing where Zn_i is more likely to be annealed out at 400 °C than O vacancies, which is due to the low diffusion energy of Zn_i; Zn_i can diffuse into

the lattice at relatively low temperature as compared with other defects.¹² The Zn_i defect density may somehow play a role on the enhanced ferromagnetism after annealing as a critical defect density will lead to optimized magnetic coupling.¹¹ It is not clear whether the easy plane ferromagnetic state in the annealed Cu-doped ZnO samples is related to single ion anisotropy as proposed by Sati *et al.*¹⁰ A theoretical calculation is sought to verify the effect of single ion anisotropy of Cu²⁺ in ZnO. It should be noted that the easy plane ferromagnetism of N1 and N2 samples is stronger than that of the thin film sample. Thus the effect of shape anisotropy in the ZnO nanoneedles at low field cannot be ruled out. Due to the ion beam bombardment, the interfacial defects and inhomogeneous distribution of Cu²⁺ ions in the nanoneedle samples are expected to be higher than that in the ZnO:Cu film. This may account for the larger changes in magnetization ratio M_s^\perp/M_s^\parallel in the nanoneedle samples than in the thin film, as interfacial defects and inhomogeneous distribution of Cu²⁺ can be removed by annealing.

In summary, an ion beam technique has been employed to dope Cu into ZnO and to make it ferromagnetic at RT. The magnetic anisotropy of the ZnO:Cu nanoneedles at high magnetic field may not be related to the shape and orientation of the nanoneedles but rather to the distribution of Cu²⁺ and defect density.

One of the authors (H.Y.Y.) acknowledges the support of Singapore Millennium Foundation Fellowships.

¹T. S. Heng, S. P. Lau, S. F. Yu, H. Y. Yang, X. H. Ji, J. S. Chen, N. Yasui, and H. Inaba, *J. Appl. Phys.* **99**, 086101 (2006).

²L. M. Huang, A. L. Rosa, and R. Ahuja, *Phys. Rev. B* **74**, 075206 (2006).

³L.-H. Ye, A. J. Freeman, and B. Delley, *Phys. Rev. B* **73**, 033203 (2006).

⁴M. H. Kane, M. Strassburg, A. Asghar, Q. Song, S. Gupta, J. Senawiratne, C. Hums, U. Habocek, A. Hoffmann, D. Azamat, W. Gehlhoff, N. Dietz, Z. J. Zhang, C. J. Summers, and I. T. Ferguson, *Proc. SPIE* **5732**, 389 (2005).

⁵Y. G. Wang, S. P. Lau, H. W. Lee, S. F. Yu, B. K. Tay, X. H. Zhang, K. Y. Tse, and H. H. Hng, *J. Appl. Phys.* **94**, 1597 (2003).

⁶S. P. Lau, H. Y. Yang, S. F. Yu, H. D. Li, M. Tanemura, T. Okita, H. Hatano, and H. H. Hng, *Appl. Phys. Lett.* **87**, 013104 (2005).

⁷X. Z. Li, *Ultramicroscopy* **99**, 257 (2004).

⁸R. D. Shannon, *Acta Crystallogr., Sect. A: Cryst. Phys., Diff., Theor. Gen. Crystallogr.* **A32**, 751 (1976).

⁹M. Venkatesan, C. B. Fitzgerald, J. G. Lunney, and J. M. D. Coey, *Phys. Rev. Lett.* **93**, 177206 (2004).

¹⁰P. Sati, R. Hayn, R. Kuzian, S. Regnier, S. Schafer, A. Stepanov, C. Morhain, C. Deparis, M. Laugt, M. Goiran, and Z. Golacki, *Phys. Rev. Lett.* **96**, 017203 (2006).

¹¹G. Bouzerar and T. Ziman, *Phys. Rev. Lett.* **96**, 207602 (2006).

¹²P. Erhart and K. Albe, *Appl. Phys. Lett.* **88**, 201918 (2006).